Journal of Biochips & Tissue Chips
ISSN: 2153-0777

Bashir et al., Biochip Tissue Chip 2016, 5:1
http://dx.doi.org/10.4172/2153-0777.1000113

Research Article Open Access

Flow Fields during Formation of W/O and O/W Emulsions using μPIV

Shazia Bashir[1,2]*, Muhammad Bashir[3], Julia M Rees[1] and Willam B Zimmerman[4]

[1]School of Mathematics and Statistics, University of Sheffield, Hicks Building, Hounsfeld Road, Sheffeld, S3 7RH, UK
[2]Department of Physics and Applied Mathematics, Pakistan Institute of Engineering and Applied Sciences, P.O. Nilore, Islamabad, Pakistan
[3]Department of Physics, COMSATS Institute of Information and Technology, Islamabad, Pakistan
[4]Department of Chemical and Biological Engineering, University of Sheffeld, Newcastle Street, Sheffeld, S1 3JD, UK

Abstract

The current work investigates two phase flow visualization in a micro channel using micron resolution particle image velocimetry (μPIV). Droplets of both oil-in-water and water-in-oil emulsions were generated in a T-shaped PDMS micro fluidic device and the corresponding flow fields were measured down-stream in the divergent section of the device. The oil-in-water emulsions were formed in a hydrophilically modified PDMS micro channel using plasma polymerization of acrylic acid. To obtain the velocity fields in both types of emulsions, fluorescent particles of 0.86 m size were added into the dispersed water phase in the case of water-in-oil emulsions, and in the continuous water phase in the case of oil-in-water emulsions. The phenomena of flow behavior within the droplets and around the droplets were investigated in detail in a diverging micro channel.

Keywords: Multiphase flow; Emulsion; Micro channel; μPIV; Droplet

Introduction

Numerous applications of microfluidic systems require a highly monodispersed droplet formation, including the biomedical industry. The behavior of a fluid at a microfluidic scale can differ significantly from that on macrofluidic scales. Typically, flow in microfluidic devices occurs at low Reynolds numbers due to the small dimension of the channels and thus is solely laminar [1,2]. Due to this laminar flow behavior, mass transfer and mixing processes occurring across adjacent fluid streams are dominated by diffusion rather than by convection [3,4]. The associated slow mixing rates can pose disadvantages for performing chemical reactions at microfluidic length scales. However, droplet based microfluidics provides a platform for fluid manipulation within the droplets. Transfer rates are increased due to the presence of high surface to volume ratios. Thus it is important to understand the hydrodynamics inside and around the droplets. Two phase flow fields at the microscale can be complicated due to surface interactions, boundary conditions or non-Newtonian rheologies. It can be di cult to adequately capture the dynamics of these effects using numerical simulations. Therefore, a non-intrusive diagnostic experimental technique such as PIV is inevitably required to analyze the flow field.

The basic principle of μPIV is same as that of conventional μPIV but in-stead the whole volume of the microchannel is illuminated. It involves an intrusion of nano to micron-sized seeding particles into the flow field. These are illuminated using a double pulsed laser. As a result, two consecutive images separated by a short time interval are recorded. These two images are then correlated to determine the displacement of particles over the time interval (separation between two images) and hence the velocity field is determined. μPIV requires an optical access to the microfluidic device and therefore the device needs to be transparent for flow visualization.

The first successful application of μPIV was made by [5] to analyze local flow fields in a microchannel. Since then, this technique has been used by a large number of researchers to characterize flow in microfluidic devices [6-11]. μPIV can be used to characterize two phase flows in a microchannel. This is particularly useful for liquid phase dispersion which is needed in the design of microreactors with enhanced performance. Generally, velocity profiles can be determined in each of the phases with the addition of appropriate seeding particles [12-15].

In this paper the flow field around an oil droplet, and inside water droplets, in a PDMS microchannel have been presented. These flow fields were analyzed at a time when the droplets had migrated far away from the T-junction and had relaxed downstream into the divergent channel. In the diverging channel fluid velocities are reduced compared to those of the initial in flow. The flow behavior differs from that in the vicinity of the T-junction. This phenomenon has not previously been well-explored, and hence it forms the basis of this study.

System Description and Principle of μPIV

As shown schematically in (Figure 1), our μPIV equipment consists

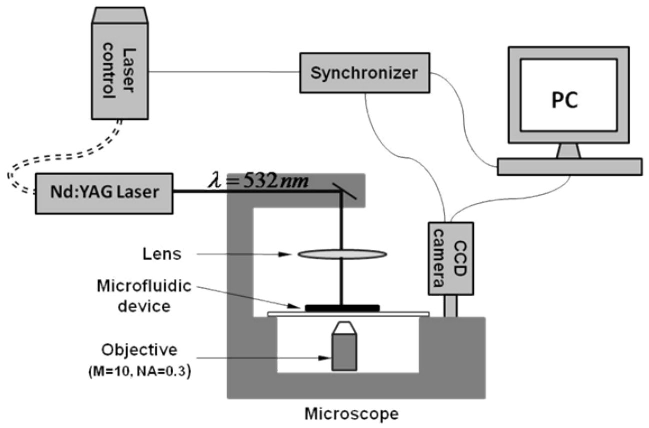

Figure 1: Schematic of experimental setup for microPIV.

***Corresponding author:** Shazia Bashir, School of Mathematics and Statistics, University of Sheffeld, Hicks Building, Hounsfeld Road, Sheffeld, S3 7RH, UK, Tel: +92-51-220-738; E-mail: shaziapieas@gmail.com

Received December 09, 2015; **Accepted** January 08, 2016; **Published** January 23, 2016

Citation: Bashir S, Bashir M, Rees JM, Zimmerman WB (2016) Flow Fields during Formation of W/O and O/W Emulsions using μPIV. J Biochips Tiss Chips 5: 113. doi:10.4172/2153-0777.1000113

of a Nd:YAG double pulsed laser with a wavelength of 532 nm. The laser is aligned with an inverted microscope (Zeiss Axiovert S100). A 12 bit CCD camera (PCO Sensicam) is mounted on the microscope for imaging with a window comprising 1280*1024 pixels. A synchronizer controls both the laser and the camera. A long pass filter with a cut o of 560 nm is used to block the laser light. A personal computer with VidPIV software installed is used to record the data and to perform the post processing of the images.

Droplet formation experiments were performed in a PDMS microfludic device consisting of a T-shaped droplet generator of 100*50 m^2 cross section, intersecting channels and a wider diverging section of 200*50 m^2 rectangular cross section where droplets are subsequently relaxed. Fluorescent particles of diameter 0.86 microns (Dukes Scienti c Co.) were used as seeding particles into the deionized (DI) water flow, which acted as a droplet phase in the case of water-in-oil emulsions and as a continuous phase in the case of oil-in-water emulsions. Mineral oil with 4% span 80 surfactant was used as an oil phase. Fluorescent particles were added into the DI water in a proportion of 30 µl per 2 ml solution (0.015% v/v). The particles were mixed into the DI water using an ultrasonic treatment for a period of 30 min duration. The laser beam illuminates a region of flow within the microchip. Fluorescent tracer particles are excited by the 532 nm wavelength laser and emit light at a wavelength of around 585 nm. A long pass filter cube adjusted below the magnification lens blocks the laser light but allows the passage of light emitted by the particles. The resulting images were acquired using a high resolution CCD camera. Pulse distance, which is the time separation between the two images was set according to the averaged flow rate of the two phase fluid flow rates in such a way that the maximum particle displacement is around 25% of the size of the interrogation window (32*32 pixels). VidPIV software computes how far the particles have moved between the pairs of images using a standard cross correlation technique and finally a map of the velocity field is generated.

Results and Discussion

µPIV measurement

Droplets are generated at a T-junction intersection and are subsequently relaxed in a divergent section of the microfluidic device [16]. The divergent section of the microchip is focused via volume illumination for PIV imaging. Flow visualization was achieved by capturing a 10-fold magnified image by the CCD camera. Therefore, the system needs to be calibrated with the actual length scale in order to determine the original distance between the particles. For this purpose, graticules with graduation marks of 0.01 mm and 0.05 mm were captured with a 10 objective lens as shown in (Figure 2). The horizontal distance with a number of pixels in a row was compared with the actual dimensions and as a result we obtained the relationship that 1 pixel=0.6667 microns. The optical parameters associated with the PIV measurements are given below in (Table 1). Hence, the field of view is 853.38 m 682.70 m for the objective lens used (Table 1). The in-plane spatial resolution of 21.3 m 21.3 m was obtained using an inter-rogation window size of 32*32 pixels. A high signal to noise ratio (SNR) is usually obtained by either reducing the depth of the channel or the particle concentration [17]. Due to the predefined dimensions of the microchannel geometries, the depth is fixed, therefore the particle concentration is the main parameter that can be optimized. The concentration of fluorescent particles in our experiment was chosen by considering results from a series of experiments comprising different particle concentrations in order to obtain adequate quality µPIV images.

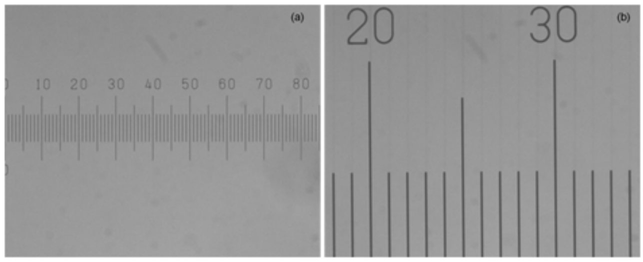

Figure 2: Graticule image with (a) 0.01 mm graduation marks and (b) 0.05 graduation marks taken by CCD camera on 10X magnification.

n (water)	M	NA	dp	p	L
Refractive index	Magnification	Numerical aperture	Particle diameter	Particle density	Wavelength
1.33	10	0.3	0.86 m	1005 kg/m³	585 nm

Table 1: Parameters for µPIV setup.

The choice of seeding particles should be made such that they are small enough to closely follow the flow and to avoid clogging of the microchannel. On the other hand they should be large enough to obtain a successful fluorescent image and to minimize the effect of Brownian motion. In contrast to fluid mechanics at macroscales, the hydrodynamic particle size is usually not of importance in microfluidics due to the large surface to volume ratios at small length scales. The particle behavior can be determined by representing the response time of a particle as a step change in fluid velocity.

Based on the assumption of Stokes flow, the response time of particles is given by:

$$\tau\rho = \frac{d_\rho^2 \rho_\rho}{18_\eta} \quad (1)$$

where d_p is the particle diameter, d_p is the density of the particle and is dynamic viscosity of the fluid. The response time of 0.86 micron diameter polystyrene particles in water, which were used in our flow visualization experiments, is of the order of 10^{-8} s which is much smaller than the time scales of any practical liquid or gas flow at low speed.

The random motion of seeding particles causes uncertainty in µPIV measurements which were quantified by Inoue [18]. The relative error, ε_B, in the measured horizontal displacement of a particle immersed in a fluid moving with velocity u, over a time interval t, is estimated as

where D is the Stokes-Einstein diffusion coefficient of a particle.

$$\varepsilon_B = \frac{1}{\mu}\sqrt{\frac{2D}{\Delta t}} \quad (2)$$

The spatial resolution of an optical system is limited by the diffraction [19]. The diameter of the diffraction limited point-spread function is given by

$$d_s = 2.44M\frac{\lambda_1}{2NA} \quad (3)$$

where M is the magnification, NA is the numerical aperture and $_1$ is wave-length of the recording light [20]. The diameter of the diffraction limited point-spread function, d_s was calculated from parameters listed in (Table 1) as 23.79 m.

The effective diameter of a particle image, d_e recorded on the CCD array is a convolution of the diffraction limited point-spread function and geometric image, and is estimated as [21,22]:

$$d_e = \sqrt{M^2 d_\rho^2 + d_s^2} \quad (4)$$

This diameter is calculated to be 25.3 m for our system. When the image on the CCD array is projected back into the flow field, the effective diameter is estimated to be 2.53 m. The diameter of the particle image needs to be resolved by more than 3-4 pixels in order to determine the location of the image correlation peak to within one tenth of the particle image diameter [23]. This results in a measurement uncertainty of $x=d_e=10M=253$ nm.

According to Meinhart [17], the measurement depth is more relevant than the depth of field in PIV. The measurement depth of two dimensional PIV is twice the distance from the objective plane in which a particle is sufficiently unfocussed that its contribution to the velocity measurement becomes insignificant. Considering this, the cut-off particle image intensity is set to be 10% of the maximum intensity of the focused particles. This gives an estimate for the total measurement depth, δz_m, as

$$\delta z_m = \frac{3n\lambda_l}{(NA)^2} + \frac{2.16 d_\rho}{\tan \theta_l} + d_\rho \quad (5)$$

where θ_l is the light collection angle of the objective [17] and n is the refractive index of water. For the current experimental setup, this value is estimated to be 25.94 m.

Flow profiles in the continuous aqueous phase during the formation of oil-in-water emulsions

A PDMS microchannel was modified from hydrophobic to hydrophilic using the atmospheric pressure plasma polymerization technique in order to form an oil-in-water emulsion [24]. Mineral oil was used as the dispersed phase and DI water was used as the continuous phase. This section analyzes the flow field around an already formed oil droplet as it flows in a divergent section of the T-junction micro fluidic device. The oil droplet formation in DI water containing fluorescent particles with 10 magnification. The base and cross µPIV images are shown in Figure 3. The velocity vectors shown in Figure 4 were obtained using the adaptive cross correlation technique. The flow profiles show that when the droplet relaxes in the divergent channel section, the continuous phase sweeps through the small gap between the oil droplet and channel walls at a higher speed due to the high shear rate existing between the continuous water phase and the droplet. Figure 5 presents the velocity pro le of the continuous water phase along the line perpendicular to the flow direction across the rear and front sides of the droplet interface, and in the middle of the droplet. The velocity is shown to be zero in the middle of oil droplet unless any particle diffusion occurs through the interface. However, fluid will flow through the gap between the oil droplet and the channel wall with a speed higher than that of droplet upstream (rear) and downstream (front) side. A gradual deceleration in the velocity profile occurs across the rear and front side of the oil droplet towards the middle of the channel due to the presence of high resistance to the flow at the interface. The magnitude of the velocity vectors in the divergent

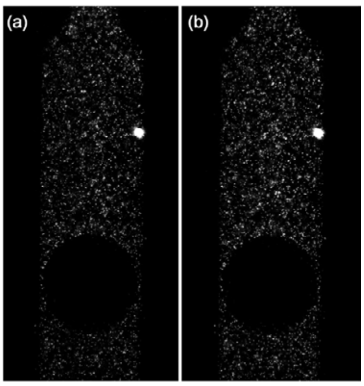

Figure 3: Fluorescent particles illuminated by the double pulsed laser in a continuous water phase that contains a previously formed oil droplet with Q_o=1 µl/min and Q_w=4 µl/min, (a) base image at time t, (b) cross image at t + 4t.

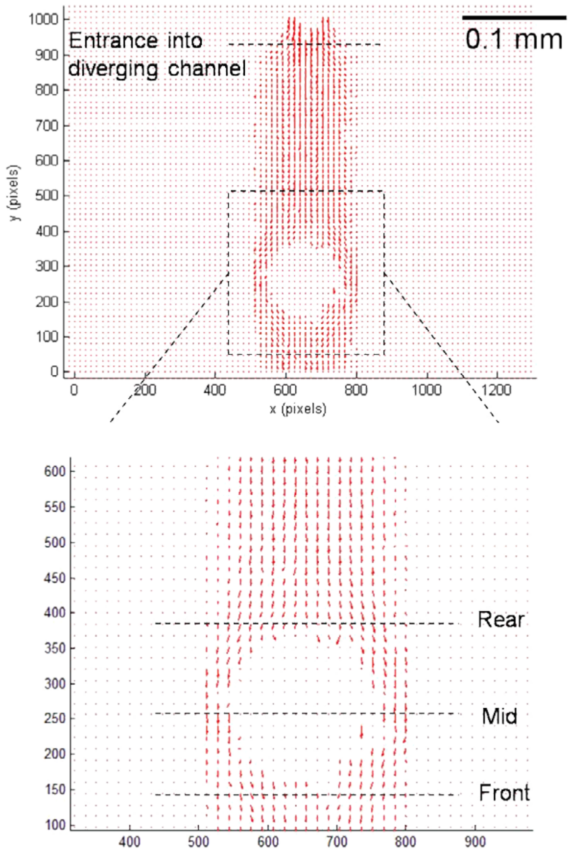

Figure 4: Velocity vectors in continuous water phase around an oil droplet, Q_o=1 µl/min, Q_w=4 µl/min.

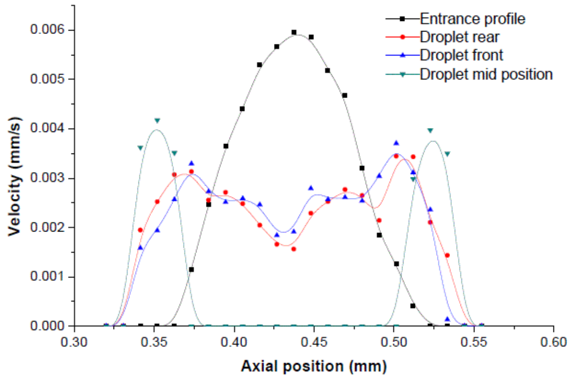

Figure 5: Velocity profiles in di erent sections of the continuous water phase around an oil droplet with Q_o=1 µl/min and Q_w=4 µl/min.

Citation: Bashir S, Bashir M, Rees JM, Zimmerman WB (2016) Flow Fields during Formation of W/O and O/W Emulsions using μPIV. J Biochips Tiss Chips 5: 113. doi:10.4172/2153-0777.1000113

channel is shown in Figure 6. The color bar indicates the lowest to highest distribution of the velocity magnitude in the channel.

Flow profiles in an aqueous droplet phase during the formation of water-in-oil droplets

The Internal flow field of a moving droplet confined in a diverging channel is presented in Figure 7. As the flow is extremely slow, we did not observe standard circulation within the droplet. As the oil flow rate increases the droplet size decreases, but still remains confined in the divergent section. It becomes unconfined at higher flow rates, e.g. at oil flow rates of 4 μl/min and 8 μl/min as shown in Figure 8, when the gap between the droplet and the wall increases. It was observed that the velocity at the stream wise interfaces for continuous phase flow rates of Q_o=0.5 μl/min, 1 μl/min and 2 μl/min is higher than those operating at flow rates of Q_o=4 μl/min and 8 μl/min (Figure 9). This is because the shear stress effect at interfaces with the continuous phase flow is more pronounced in the case of confined droplets. The velocity profile is slightly parabolic in the case of the lowest flow rate considered (Q_o=0.5 μl/min), showing that in the center of the droplet the flow is weakly accelerated. This profile damps gradually at increasing continuous phase flow rates and eventually becomes reversed within the unconfined droplet at highest flow rate considered (8 μl/min), showing a strong deceleration in the center of droplet. However, the overall motion of the droplet follows the direction of flow downstream.

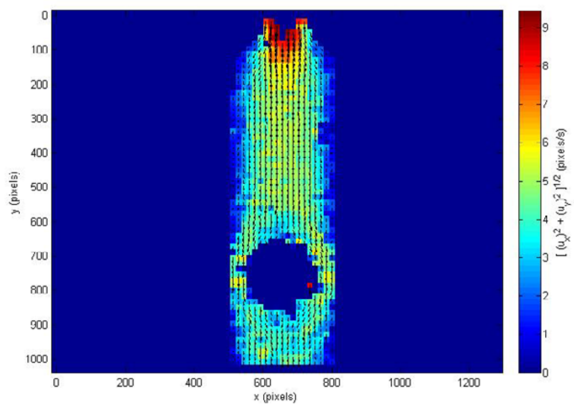

Figure 6: Velocity profiles in continuous water phase containing an already formed oil droplet, Q_o=1 μl/min, Q_w=4 μl/min.

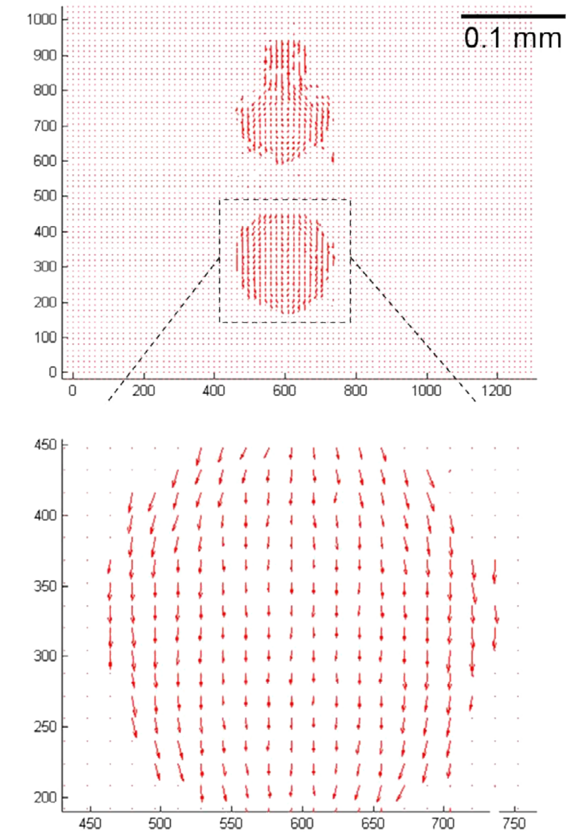

Figure 7: Velocity Vectors in continuous water phase around an oil droplet, Q_o=1 μl/min, Q_w=1 μl/min.

Conclusions

The flow profiles presented herein provide a fundamental understanding of the very slow flow rate of droplets within a divergent microchannel. The flow becomes very slow as the droplets move downstream in the divergent section of the microchannel. These results in the velocity profiles across water droplets dispersed in a carrier oil indicating that no regions of circulation are present. Furthermore, flow profiles in the center of water droplet for different flow rates were compared and it was found that the degree of confinement of the droplet in the divergent microchannel altered the velocity profiles in droplets. The flow was observed to decelerate through the thicker films

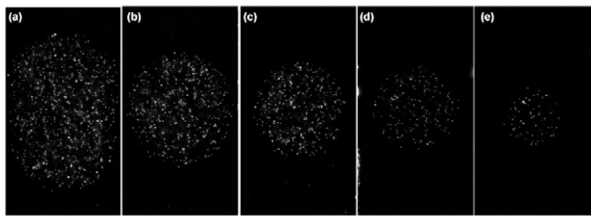

Figure 8: PIV images of fluorescent particles in water droplet moving in diverging section of microchannel at different oil flow rates of (a) Q_o=0.5 μl/min, (b) Q_o=1 μl/min, (c) Q_o=2 μl/min, (d) Q_o=4 μl/min, (e) Q_o=8 μl/min.

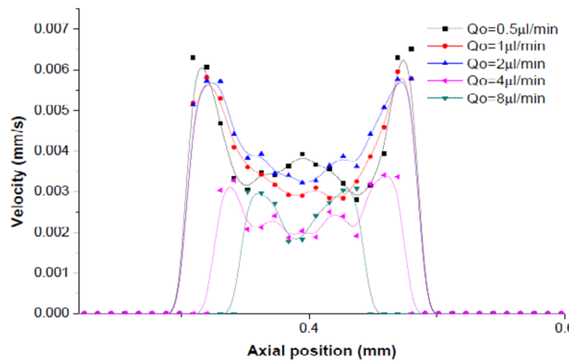

Figure 9: Velocity profiles across water droplets dispersed in a continuous oil phase for range of flow rates Q_o=0.5 μl/min, 1 μl/min, 2 μl/min, 4 μl/min and 8 μl/min with a constant dispersed water phase flow rate of Q_w=1 μl/min. The profiles are shown in mid position of the droplet perpendicular to the flow direction.

of carrier fluid that existed between the droplet and the microchannel walls. In the case of the formation of an oil-in-water emulsion, velocity profiles in the continuous water indicated that the maximum velocity occurred around the interface adjacent to the channel wall. This arose due to the strong shear existing between the droplet and the channel wall. A high degree of deceleration in the flow around the center of the rear interface of the oil droplet was observed which is due to the high level of resistance to the flow, and around the center of the front interface due to the resistance to the out flow. Hence, it was concluded that the degree of mixing occurring within the droplets in two phase flow may not always be as strong as previously reported due to the zero velocity gradients that appear at lower velocities and also due to the droplet travelling in an area of lower velocity gradients due to thickening of the thin lm in the diverging channel surrounding the droplet. Our methodology has accurately predicted when the flow within a droplet will be non-circulatory. This could be validated numerically using computational fluid dynamics with the conditions of the physical properties and flow rates imposed. Such simulations can be used to determine the optimum velocities at which the flow will start to circulate inside the droplet. Our µPIV technique enables the local flow field analysis at high spatial resolution. However, this technique is limited by several factors including particle size, image quality and density of seeding particles.

Acknowledgments

Authors acknowledge support from the EPSRC grant EP/E01867X/1 (Bridging the Gap between Mathematics, ICT and Engineering Research at Sheffeld). The authors would like to acknowledge EPSRC grants GR/S08695 and EP/I019790/1 for supporting the microPIV facility. We also thank to Dr. Bandulasena for helpful discussions.

References

1. Teh SY, Lin R, Hung LH, Lee AP (2008) Droplet microfluidics. Lab Chip 8: 198-220.
2. Squires TM, Quake SR (2005) Micro fuidics: Fluid physics at the nano-liter scale. Reviews of Modern Physcis 77: 977-1026.
3. Stone HA, Stroock AD, Ajdari A (2004) Engineering flows in small devices: microfuidics toward a lab-on-a-chip. Annu Rev Fluid Mech 36: 381-411.
4. Figeys D, Pinto D (2000) Lab-on-a-chip: a revolution in biological and medical sciences. Anal Chem 72: 330A-335A.
5. Santiago JG, Wereley ST, Meinhart CD, Beebe DJ, Adrian RJ (1998) A particle image velocimetry system for microuidics. Experiments in Fluids 25: 316-319.
6. Devasenathipathy S, Santiago JG, Wereley ST, Meinhart CD, Take-hara K (2003) Particle imaging techniques for microfabricated uidic systems. Experiments in Fluids 34: 504-514.
7. Sinton D (2004) Microscale flow visualization, Microfluidics Nanofluidics 1: 2-21.
8. Bown MR, MacInnes JM, Allen RWK, Zimmerman WBJ (2006) Department of three-dimensional, three-component velocity measurements using stereoscopic micro-PIV and PTV. Meas Sci Technol 17: 2175-2185.
9. Lindken R, Westerweel J, Wieneke B (2006) Stereoscopic micro particle image velocimetry. Experiments in Fluids 41: 161-171.
10. Bandulasena HCH, Zimmerman WB, Rees JM (2008) An inverse methodology for the rheology of a power law non-Newtonian fluid. Journal of Mechanical Engineering Science Part C 222: 761-768.
11. Bandalusena HCH, Zimmerman WB, Rees JM (2009) Microuidic rheometry of a polymer solution by micron resolution particle image velocimetry: A model validation study. Meas Sci Technol 20: 115404.
12. Van Steijn V, Kreutzer MT, Kleijn CR (2007) µPIV study of the formation of segmented flow in microfluidic T-junctions. Chem Eng Sci 62: 75057514.
13. Malsch D, Gleichmann N, Kielpinski M, Mayer G, Henkel T (2010) Dynamics of droplet formation at T-shaped nozzles with elastic feed lines. Microfluid Nanofluid 8: 497-507.
14. Timgren A, Tragardh G, Tragardh C (2008) Application of the PIV technique to measurements around and inside a forming drop in a liquid-liquid system. Exp Fluids 44: 565-575.
15. Wang C, Nguyen NT, Wong TN (2007) Optical measurement of flow field and concentration field inside a moving nanoliter droplet. Sensors and Actuators A 133: 317-322.
16. Bashir S, Solvas XC, Bashir M, Rees JM, Zimmerman WBJ (2014) Dynamic wetting in microuidic droplet formation. Bio Chip Journal 8: 122-128.
17. Meinhart CD, Wereley ST, Gray MHB (2000) Volume illumination for two-dimensional particle image velocimetry. Meas Sci Technol 11: 809-814.
18. Inoue S, Spring RK (1997) Video Microscopy: The Fundamentals. (2ndedn), Plenum Press, New York.
19. Nguyen MT, Wereley ST (2006) Fundamentals and applications of microuidics. Artech House Inc.
20. Adrian RJ, Yao CS (1985) Pulsed laser technique application to liquid and gaseous flows and the scattering power of seed materials. Appl Opt 24: 44-52.
21. Adrian RJ (1997) Dynamic ranges of velocity and spatial resolution of particle image velocimetry. Meas Sci Technol 8: 1393-1398.
22. Prasad AK, Adrian RJ, Landreth CC, Offutt PW (1992) Effects of resolution on the speed and accuracy of particle image velocimetry inter-rogation. Experiments in Fluids 13: 105-116.
23. Bashir M, Bashir S, Rees J, Zimmerman M (2014) Surface coating of bonded PDMS microchannels by atmospheric pressure microplasma. Plasmna Processes and Polymers 11: 279-288.
24. Bashir M, Bashir S (2015) Hydrophobic-hydrophilic character of hexamethyldisiloxane films polymerized by atmospheric pressure plasma jet. Plasma Chemistry and Plasma Process 35: 739-755.

Citation: Bashir S, Bashir M, Rees JM, Zimmerman WB (2016) Flow Fields during Formation of W/O and O/W Emulsions using µPIV. J Biochips Tiss Chips 5: 113. doi:10.4172/2153-0777.1000113